Korean J. Chem. Eng., **30**(10), 1904-1910 (2013)
DOI: 10.1007/s11814-013-0130-8

Surface chemistry and adsorption mechanism of cadmium ion on activated carbon derived from *Garcinia mangostana* shell

Yee Li Kang*, Mei Yi Poon*, Purushothaman Monash, Shaliza Ibrahim*, and Pichiah Saravanan*,†**

*Environmental Engineering Laboratory, Department of Civil Engineering, University of Malaya, Kuala Lumpur 50603, Malaysia
**Department of Chemical Engineering, University of Malaya, Kuala Lumpur 50603, Malaysia
(*Received 23 January 2013 • accepted 17 July 2013*)

Abstract−A detailed surface characterizations and adsorption mechanism of Cd^{2+} on chemical activated carbon (CAC) prepared from *Garnicia mangostana* shell were investigated. The activation is accomplished in self-generating atmosphere using phosphoric acid as activating agent. The characterizations performed are elemental analysis, functional group identification, N_2 adsorption isotherm and surface charges. Adsorption mechanism of metal ion was tested using Cd^{2+} as model ion. CAC achieved BET surface area of 1,498 m^2/g with a mixture of micro and mesopores. The point of zero charge is observed to be at pH 2.8 and the optimum pH for Cd^{2+} adsorption on CAC is 12. The adsorption isotherm followed the Freundlich model, and the adsorption kinetics was explained by pseudo-second order kinetic model. From thermodynamic studies, the adsorption was found to be physical adsorption. X-ray photoelectron spectroscopy (XPS) confirmed the adsorption of Cd^{2+} onto CAC as +2 oxidation state.

Key words: *Garcinia mangostana*, Activated Carbon, Adsorption Mechanism, Surface Chemistry

INTRODUCTION

Due to the drastic increase in electronics based and electroplating manufacturing industries, more and more heavy metal compounds are mined, used and released into the aquatic water bodies. At present, numerous treatment methods such as flocculation, coagulation, ion exchange, chemical precipitation, filtration, and adsorption are practiced for heavy metals removal [1,2]. Adsorption using activated carbon (AC) is one of the most popular treatment techniques due to its easy handling and sustainability. However, the increasing cost of commercial AC is hindering the development of this technology [3]. Hence, in recent years many researchers have focused on finding suitable and economical adsorbents especially from plant biomass and biomaterial waste [1,4-6]. Agricultural wastes that are widely available and economical are the most suitable precursor for production of such AC in large quantity.

Garnicia mangostana, commonly known as mangosteen, is a fruit known for its remedial properties that is used as alternative medicine [5]. Recently, there has been an increased interest in this fruit in the food and beverage industries, causing the massive generation of mangosteen shells commercially. To address this issue, few researchers have reported the use of mangosteen shell as precursor for AC using K_2CO_3 as activating agent with promising results [5,7]. High fixed carbon and low ash content of this shell makes it a suitable raw material for AC as found by Chen et al. [5]. However, the research on activating mangosteen shells using phosphoric acid is scant.

In the adsorption process, a detailed understanding of metal binding mechanisms with active sites facilitates the determination of the rate-limiting step. Such information is important for the rational design and optimization of the adsorbents and adsorption conditions. However, study pertaining to the role of surface chemistry and the adsorption mechanism is limited. Thus the focus of the present work is to analyze the surface characteristics of mangosteen shell, before and after treatment, and their role in solid-liquid adsorptions, using Cd^{2+} as a model compound.

†To whom correspondence should be addressed.
E-mail: pichiahsaravanan@gmail.com

MATERIAL AND METHODS

1. Preparation of Sample

Mangosteen shell (MS), an agricultural waste, is used as the precursor for the production of AC in this study. Initially, the MS was cleaned and air-dried to remove dirt and other impurities. For the production of char sample, the MS was crushed into small pieces (≈1 cm) and was directly burned without acid impregnation at 773 K for 1 h in a muffle furnace. The chemically activated carbon (CAC) was activated using the methods reported in our previous work [8]. The activation was done using single stage phosphoric acid (H_3PO_4) activation in self-generated atmosphere. Briefly, the MS were ground and sieved to obtain powder in the size of ≤1 mm (18 mesh size) before being impregnated with 85% H_3PO_4 (1 : 1 weight ratio). The slurry was then burned at 673 K under self-generated atmosphere in a muffle furnace. The product was washed in 1% $NaHCO_3$ to achieve neutral pH. All samples were ground and sieved into ≤1 mm before subsequent testing and analysis. The average particle size of MS, char and CAC used was 1.21 mm, 0.65 mm and 0.51 mm, respectively, as evaluated by Zetasizer Nano particle size analyzer (Malvern Instrument Ltd., UK) (Fig. S1(a)-(c)). The yield of the char and CAC was 21% and 47%, correspondingly.

2. Preparation of Synthetic Cd^{2+} Solution

A stock solution of cadmium ion (Cd^{2+}) (1,000 mg/L) was prepared by dissolving appropriate quantity of cadmium nitrate salt, $Cd.N_2.O_6.4H_2O$ (Sigma-Aldrich) in deionized water. The stock solu-

tion was then suitably diluted to required concentrations in the following investigations.

3. Characterization of Samples

The CHN analysis of all samples was verified by using an elemental analyzer (Perkin Elmer 2400) and functional groups were identified by Fourier transform infrared spectrometer (FT-IR) (Thermo Scientific Nicolet iS10 FTIR) in the range of 500-4,000 cm^{-1}. The surface morphology was observed using field emission scanning electron microscope (FESEM) (Hitachi SU8000 SP), and X-Ray diffraction (XRD) patterns were recorded by the Siemens D5000 powder X-Ray diffractometer for crystallinity check.

Surface charges were examined by point of zero charge (pH_{pzc}) at 298 K. The pH_{pzc} was determined as described by Foo and Hameed [7]. The pH of 0.01 M NaCl (100 mL) was varied in the range of pH 2 to 12. Sample, amounting to 0.3 g, was added into the solution and shaken for 48 h. The final pH of the NaCl solution was measured and the point of zero charge was identified at the point where initial pH is equivalent to the final pH.

The N_2 adsorption-desorption isotherms for all three samples were measured using Quantachrome's AUTOSORB-6B surface area and pore size analyzer at 77 K. Prior to analysis, the samples were outgassed at 423 K for 5 h to remove the existing moisture. The isotherms data obtained were used to classify the textural parameters of the samples, including surface area, pore volume and pore size using appropriate models.

X-ray photoelectron (XPS) analysis was done with KRATOS Axis Ultra DLD for char and CAC samples to validate the results of elemental and functional group analysis.

4. Batch Adsorption Experiments

Adsorption experiments were performed in batch mode for CAC. The batch experiments were carried out at fixed dosage (0.05 g/100 mL). The mixture was shaken in an incubator shaker (Daihan LabTech) at 200 rpm. Other environmental conditions of the experiments were not adjusted unless stated. The isotherm and kinetic studies were performed by varying the initial concentration of Cd^{2+} from 10 to 50 mg/L for different time interval up to 6 h at pH 5.6. The effect of pH on adsorption capabilities was observed by altering the pH in the range of 2 to 12 using 20 mg/L of Cd^{2+} as initial concentration at 303 K. The pH was adjusted using 0.1 M H_2SO_4 or NaOH solution and measured using Mettler Toledo FE20. For thermodynamic study, the temperature was adjusted in the range 303, 310 and 320 K. The thermodynamic parameters were calculated using the van't Hoff equation. The residue concentration of Cd^{2+} was measured by ICP-OES (Perkin Elmer, Optima 3000).

RESULTS AND DISCUSSION

1. Elemental Analysis, Morphology and Crystallinity

The CHN analysis of the samples is tabulated in Table 1. The

Table 1. CHN element analysis of MS, char and CAC

Element (wt%)	MS	Char	CAC
C	39.28	53.18	35.23
O	54.83	42.37	59.82
H	5.11	3.57	4.48
N	0.78	0.88	0.47

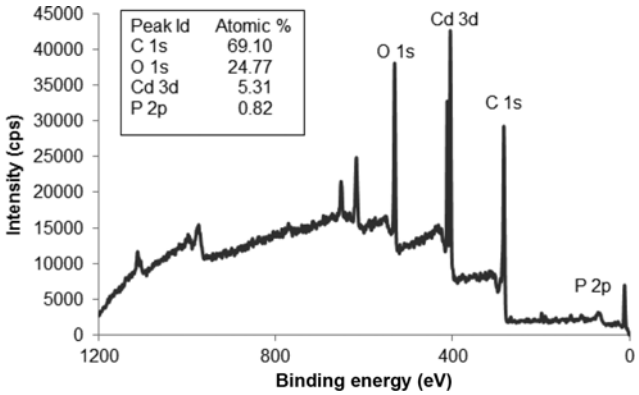

Fig. 1. XPS wide spectrum for CAC after Cd^{2+} adsorption.

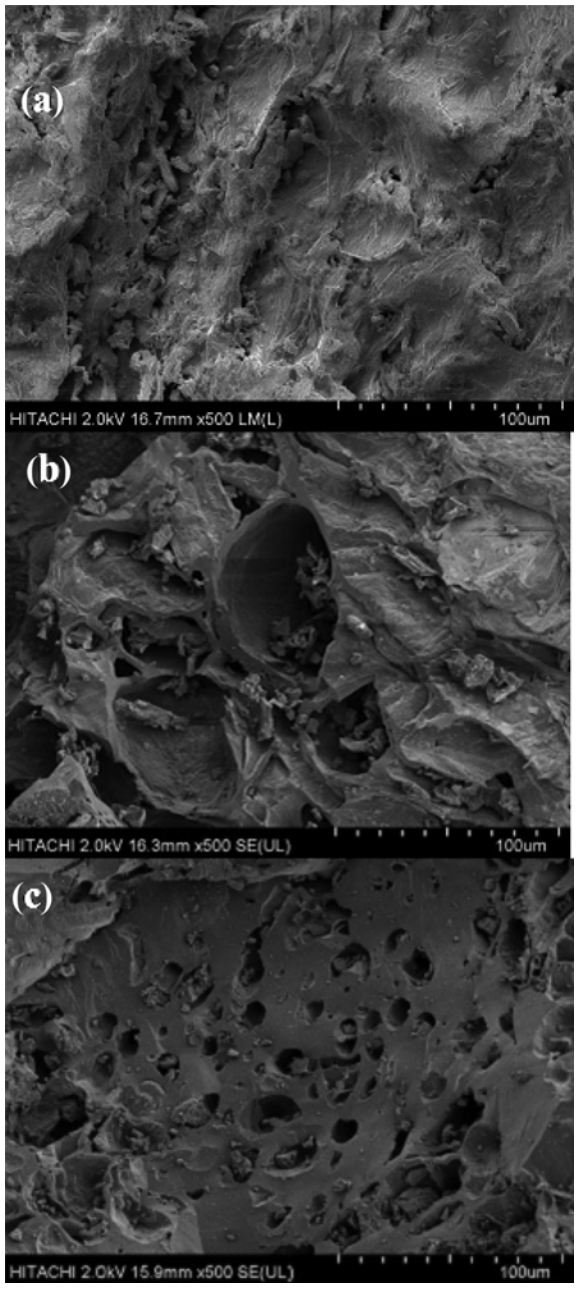

Fig. 2. FESEM micrographs of (a) MS, (b) char and (c) CAC.

analysis gives a stoichiometric analysis of the samples using combustion technique. The analysis for MS is consistent with that found in previous research [5]. The content of carbon (C) for char increased but decreased for CAC. Phosphorus element was detected in CAC from wide spectrum XPS analysis (Fig. 1) due to the impregnation of phosphoric acid during preparation stage. The FESEM images of MS, char and CAC are shown in Fig. 2(a)-(c). It can be observed that prior to treatment, the precursor had fibrous surface with no discernible pores on it. For char sample, large aperture can be seen on the surface, while more regular pores are observed on the surface of CAC. Comparison between these three micrographs demonstrates the role of H_3PO_4 in assisting a more controlled pore formation during activation. The pore size and distribution is further discussed in the later part of this section under surface area characterization.

The XRD pattern in Fig. S2 indicates the presence of amorphous carbon in all three samples. Graphitization occurred after treatment as char and CAC register a minor peak at ~43° indicative of (1 0 0) plane graphite.

2. Functional Group Analysis

FT-IR and XPS analysis are used to identify functional groups in the samples. FT-IR spectra for MS, char and CAC are shown in Fig. 3. The FT-IR spectrum of MS plotted similar peaks as reported

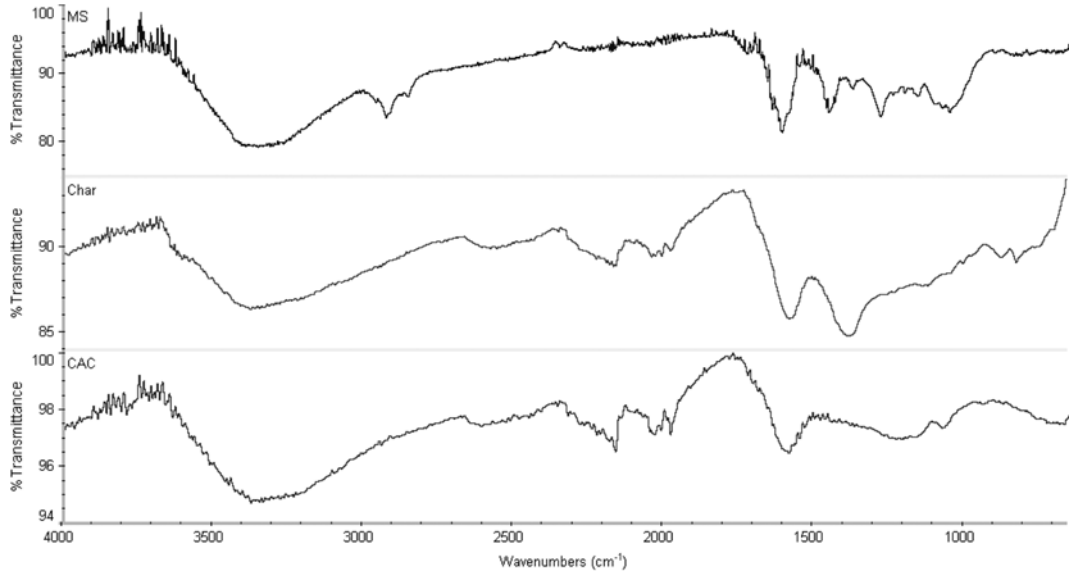

Fig. 3. FT-IR spectrum for MS, char and CAC.

Table 2. Deconvolution results of XPS spectra of CAC and char

Sample	Region	Peak	Position (eV)	FWHM (eV)	Mass concentration (%)	Assignment
CAC	C 1s	A	282.5	1.5	10.21	C-O
		B	283.5	1.5	23.03	Carbide
		C	284.7	1.5	53.66	Graphite
		D	286.7	1.5	6.87	C=O
		E	288.7	1.5	6.23	COOH/-C-(O)-O-
	O 1s	A	529.6	1.1	12.42	Metal oxide
		B	530.6	0.9	17.62	=O
		C	531.4	1.3	47.05	CdO
		D	532.5	1.1	14.99	-O-/$Cd(OH)_2$
		E	533.2	1.1	7.92	-OH/COOH/-C-(O)-O-
	Cd 3d	A	404.4	1.4	15.27	CdO
		B	405.6	1.6	45.01	Cd/$Cd(OH)_2$
Char	C 1s	A	284.5	1.5	72.91	Graphite
		B	285.5	1.7	27.09	COOH/C-(O)-C
	O 1s	A	530.5	1.1	12.72	=O for carbonyl/carboxyl group
		B	531.6	1.2	18.79	
		C	532.6	1.1	33.36	-O-
		D	533.5	1.1	18.98	alcohol/carboxylic acid/ester
		E	534.4	1.4	16.15	carboxyl groups/ester/ether

Source: NIST X-ray photoelectron spectroscopy database, http://srdata.nist.gov/xps/

by previous studies [5,9]. Broad bands at 3,400-3,250 cm^{-1} indicate the presence of -OH functional groups, and the doublet peaks at 2,916 cm^{-1} and 2,850 cm^{-1} account for the stretching vibration C-H groups [9,10]. The presence of carbonyl and carboxyl late ions (C=O/COO-) can be explained from the presence of a strong peak at 1,602 cm^{-1} and a weaker peak at 1,442 cm^{-1} [9-11]. The bands at 1,275 and 1,046 cm^{-1} are due to O-C stretching of the ether group and the alcoholic groups, which may also indicate the presence of lignin structure (C-O-C and -OCH_3) [9,11]. The reduction and disappearance of many peaks in char and CAC sample compared to MS spectrum indicate the conversion of certain functional groups into volatile matter as a result of high temperature and chemical reaction [5]. Some of the functional groups that are still present, albeit in reduced intensity in CAC, are -OH (3,400-3,250 cm^{-1}), C=O/COO- (1,590-1,620 cm^{-1}) and O-C (1,060 cm^{-1}) groups. The spectrum for CAC also showed an additional peak at 1,234 cm^{-1}, indicating the presence of phosphonate, P=O functional group. This group is attached to the CAC during the H_3PO_4 activation. For char sample, the presence of -OH (3,380 cm^{-1}) and carbonyl/carboxyl (C=O/COO-) (1,580-1,390 cm^{-1}) groups is detected but O-C group is no longer detected from the spectrum.

A summary of the spectra deconvolution of XPS is tabulated in Table 2. The deconvolution of high resolution C 1s spectrum of CAC shows the presence of oxide (peak A), carbide (peak B) and graphitic carbon (peak C) [12]. Carbon in carbonyl groups and carboxyl and/or ester groups are identified on peaks D and E, respectively [12]. However, peaks D and E contribute less than 15% of the total carbon content. This is in agreement with the significantly reduced intensity of peaks representative of carboxylate ions and lignin groups in FT-IR. The analysis of O 1s spectra for CAC implies the presence of carbonyl, carboxyl, ester and alcohol groups (=O and -O-). Only two carbon species are identified in char, with graphite (peak A) as major carbon component and carbon (peak B) in carboxylic acid and/or ether groups as minority. The deconvolution of O 1s spectrum for char sample points towards the presence of carboxylic acid and its derivatives, which is parallel to FT-IR findings.

Oxide and hydroxide of Cd are also detected on the O 1s (531.4 and 532.5 eV) and Cd 3d (404.4 and 405.6 eV, respectively) spectra for CAC as listed in Table 2. This establishes that the oxidation state of Cd ions involved in adsorption is +2. The XPS spectrum for Cd 3d is shown in Fig. S3.

3. Surface Area Characterization

Adsorption-desorption isotherm provides both qualitative and quantitative insight to adsorption mechanism and pore characteristics of an adsorbent [5,13]. N_2 adsorption and desorption isotherm data can be used for various models to determine the surface characteristics of the adsorbents. There are different types of isotherms classified by the IUPAC system and each isotherm represents a different nature of adsorption process [14]. Types of isotherm give an understanding on the pore size and shape of the material. Type I indicates monolayer adsorption on microporous solids, while Type III results by multilayer adsorption. Type II isotherm demonstrates both monolayer and multilayer adsorption. Type IV and V isotherms are a derivation of Type II and III isotherms, respectively, with the occurrence of hysteresis,signifying capillary condensation [14]. For MS, the isotherm shown in Fig. 4(a) fits the Type III isotherm of the IUPAC classification, which has extremely weak adsorbate-adsorbent interaction [14]. This type of isotherm is not applicable in the BET model. The t-plot resulted in nil micropores for the MS (Fig. S4). From BJH and DFT models, pore volume detected in the range of mesopores is also negligible. This result is consistent with the dense and non-porous surface of MS shown in FESEM micrograph in the previous section. For char, the isotherm (Fig. 4(b)) is also a Type III isotherm similar to the isotherm obtained for MS [14]. The volume of gas adsorbed is very low (0-5 cm^3/g), revealing that the pores formed are shallow. The obtained hysteresis denotes the presence of capillary condensation, which in general is not suitable for adsorption. The isotherm for CAC depicts a mixture of Type I and Type II isotherm, consisting of a mixture of micro and mesopores (Fig. 4(c)). The isotherm obtained was similar to the AC prepared by K_2CO_3 activation using microwave with the same precursor [7]. The obtained pore size distribution by HK and BJH method confirms the presence of micro (0.6-2.0 nm) and meso (2.2 nm) pores, as shown in Figs. S5 and S6. In addition, it is further verified with DFT model and the pore size is found to be in the range between 0.4 and 4.7 nm (Fig. S7). The surface area and pore volume

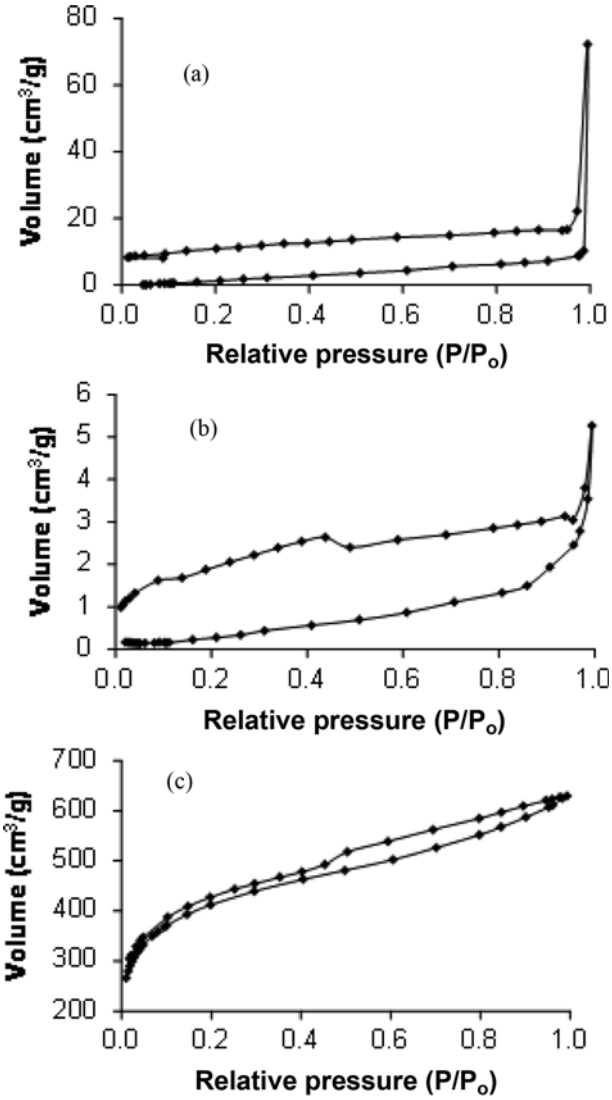

Fig. 4. N_2 adsorption-desorption isotherm (a) MS, (b) char and (c) CAC.

Table 3. Comparison of porosity characteristics of various AC by *Garcinia mangostana* using different activation methods

Activation method	S_{BET} (m^2/g)	S_{mic} (m^2/g)	V_t (cm^3/g)	V_{mic} (cm^3/g)	D (nm)	Ref.
Two-stage activation in self-generated atmosphere using K_2CO_3 as activating agent	1123	908	0.56	0.45	1.98	5
Two-stage activation in inert atmosphere using K_2CO_3 as activating agent in microwave assisted activation	1099	626	0.61	0.33	2.23	7
One-stage activation in self-generated atmosphere using H_3PO_4 as activating agent	1498	1683	0.94	0.60	2.51	Present study

S_{BET}: BET surface area; S_{mic}: micropore area; V_t: total pore volume; V_{mic}: micropore volume; D: average pore diameter

of the CAC are found to be 1,498 m^2/g and 0.939 cm^3/g, respectively. The high surface area signifies the presence of abundant active sites. The surface characteristic of CAC is compared with AC of similar raw material and presented in Table 3. The prepared CAC recorded the highest surface area and total pore volume than that of the others. From Table 3, it is evident that the present preparation method is superior to other reported methods.

4. Isotherm Studies

The optimization of design for adsorption system importance can be established through isotherm models [15]. The adsorption capacity and equilibrium characteristics of CAC for the adsorption of Cd^{2+} are measured by using the Langmuir, Freundlich and Temkin isotherm models in this study. The linearized equations for these isotherm models are as follows, respectively:

$$\frac{C_e}{q_e} = \frac{1}{Q_0 b} + \frac{1}{Q_0} C_e \quad (1)$$

$$\ln q_e = \ln K_F + \frac{1}{n} \ln C_e \quad (2)$$

$$q_e = \frac{RT}{b} \ln K_T + \frac{RT}{b} \ln C_e \quad (3)$$

where C_e (mg/L) is the equilibrium concentration, q_e (mg/g) amount adsorbed per amount of adsorbent, b (L/mg) amount of adsorbate required to form a monolayer and Q_0 (mg/g) are Langmuir equilibrium constant [16]. The constant K_F (mg/g) is an indication of the multilayer adsorption capacity and 1/n is related to adsorption intensity for the Freundlich isotherm model [17]. The value of 1/n ranging from 0 to 1 indicates the degree of surface heterogeneity. The surface is said to be more heterogeneous as the value approaches 0 [17]. Temkin isotherm parameter, K_T (L/mg) represents Temkin equilibrium binding constant, while b (J/mol), R (8.314 J/mol K) and T (K) are Temkin constants related to equilibrium binding constant, gas constant and absolute temperature, respectively.

The Langmuir isotherm assumes complete monolayer adsorption occurring on homogeneous adsorption sites and used to evaluate maximum adsorption capacity. Conformation of the Langmuir isotherm indicates the adsorption sites are equivalent in terms of energy and homogeneous surface. A separation factor, R_L can be further derived from the Langmuir equation, given by the following equation:

$$R_L = \frac{1}{(1 + b(C_0))} \quad (4)$$

where C_0 is the initial concentration. When the value of R_L is between 0 and 1, it indicates favorable adsorption, while the adsorption process is unfavorable if R_L>1. While R_L=0 indicates irreversible adsorption, R_L=1 represents linear adsorption [16]. The Freundlich isotherm is applied to multilayer adsorption onto heterogeneous surface with irregular distribution of adsorption energy and affinity. The Temkin isotherm assumes the heat of adsorption decreases linearly with surface coverage of adsorbent due to sorbate/sorbent interactions.

Table 4. Isotherm parameters for Cd^{2+} adsorption on CAC

Isotherms	Parameters	Values
Langmuir	Q_0 (mg/g)	35.97
	b (L/mg)	0.032
	R^2	0.652
Freundlich	K_F (mg/g) (L/mg)$^{1/n}$	1.208
	n	11.145
	R^2	0.992
Temkin	K_T (L/mg)	0.931
	B	3.601
	R^2	0.931

The adsorption equilibrium data for Cd^{2+} on CAC was fitted into the three models and evaluated using a correlation coefficient, R^2. A summary of the parameters is listed in Table 4. The adsorption of Cd^{2+} on CAC is best represented by the Freundlich isotherm with highest R^2 value of 0.992. This indicates that the surface of CAC is not uniform and adsorption sites were heterogeneous. The adsorption process is favorable as the R_L value (0.755) is less than 1.

5. Kinetic Studies

The rate of adsorption process can be determined by using kinetic models. Two kinetic models, pseudo-first order and pseudo-second order kinetics, were used in this study. The equations of both models are listed below:

$$\ln(q_e - q_t) = \ln(q_e) - (k_1)t \quad (5)$$

$$\frac{t}{q_t} = \left(\frac{1}{k_2 q_e^2}\right) + \left(\frac{1}{q_e}\right)t \quad (6)$$

where q_e and q_t (mg/g) are the amount of adsorbate adsorbed per unit weight of adsorbent at equilibrium and at any time t, respectively, k_1 (1/h) is the rate constant for pseudo-first order model, while k_2 (g/mg h) is the rate constant for pseudo-second order kinetic model. A normalized standard deviation, Δq, was used to quantify the fitness of these models to the experimental data by using the following equation:

Table 5. Parameter for kinetic models for Cd^{2+} adsorption on CAC

	Initial concentrations (mg/L)				
	10	20	30	40	50
q_{exp} (mg/g)	1.706	3.352	4.919	7.122	8.446
Pseudo-first-order					
K_1 (min^{-1})	0.016	0.011	0.030	0.016	0.029
q_{calc} (mg/g)	0.802	0.462	7.626	2.277	9.638
R^2	0.417	0.528	0.528	0.600	0.762
Δq (%)	18.28	33.04	26.08	35.46	32.55
Pseudo-second-order					
K_2 (g/mg·min)	0.0232	0.0193	0.0063	0.0070	0.0044
q_{calc} (mg/g)	1.593	3.022	5.316	6.671	8.850
R^2	0.904	0.942	0.939	0.975	0.981
Δq (%)	2.78	4.00	3.29	2.57	1.93

$$\Delta q(\%) = 100 \times \sqrt{\frac{\sum[(q_{exp} - q_{calc})/q_{exp}]^2}{n-1}} \quad (7)$$

where q_{exp} and q_{calc} refer to experimental data and calculated values and n is the number of data points. Smaller values of Δq signify a better fit.

The detailed parameters of these models are tabulated in Table 5. The low values of Δq obtained for pseudo-second order kinetics indicate that the experimental q values did not deviate much from the calculated values. The correlation coefficients, R^2, for the pseudo-second order kinetic model ranged from 0.92 to 0.98 compared to pseudo-first order, which ranged between 0.42 and 0.76. Based on the two analyses, the adsorption kinetics of Cd^{2+} onto CAC is better described by pseudo-second order kinetic model.

6. Thermodynamic Study

Thermodynamic parameters, change in standard enthalpy (ΔH^o), change in standard entropy (ΔS^o) and change in Gibbs free energy (ΔG^o), are calculated in this study using the van't Hoff equation:

$$\ln K_d = \frac{\Delta S^o}{R} - \frac{\Delta H^o}{RT} \quad (8)$$

$$\Delta G^o = -RT \ln K_d \quad (9)$$

where R is the universal gas constant (8.314 J/mol K), T (K) is the absolute temperature and K_d is the distribution coefficient. From Eq. (8), ΔH^o and ΔS^o are obtained from the gradient and y-intercept of ln K_d versus 1/T plot. The ΔG^o values are found to be 1.721, 1.504 and 1.287 kJ/mol at 303, 313 and 323 K, respectively. The lower value of positive ΔG^o suggests that adsorption is feasible and not spontaneous [18]. The low positive ΔH^o (8.3 kJ/mol) value suggests the adsorption is physical [19]. The positive ΔS^o (21.7 J/mol) is attributed to increased randomness.

7. Surface Chemistry

Surface charge is an important factor influencing the adsorption process and mechanism. The type of adsorbate suitable for a particular adsorbent mainly depends on this factor. pH is an important variable influencing the adsorption mechanism, especially for heavy metal ions as it alters the type of ionic species present and their degree of ionization in the adsorbate and also the net charges on the surface of the adsorbent [20-22]. The effect of pH on the surface charge can be done experimentally and by point of zero charge (pH_{pzc}). The net surface charge of the material will remain positive for any pH below pH_{pzc} and vice versa [7]. The pH_{pzc} for CAC is 2.8. Experimentally, Cd^{2+} solution was prepared over a pH range of 2-12 and the resulting adsorption capacity is shown in Fig. 5. Hence, the CAC is negatively charged throughout the studied pH except for pH 2. The lower percentage removal of Cd^{2+} observed at pH 2 is attributed to the electrostatic repulsion between the positively charged CAC and positively charged Cd^{2+} metal ions. When the pH is increased from 4 to 12, the electrostatic attraction between the CAC and Cd^{2+} increases, attributed to the negative surface charge of the CAC after pH is greater than 2.8. However, a decreased percentage removal found at pH 6, due to the formation of $Cd(OH)^+$ during pH adjustment, is attributed to the competitive adsorption between the positively charged metal cations (Cd^{2+} and $Cd(OH)^+$) with the negatively charged CAC adsorbent. In general, when the pH is increased to above 7, the $Cd(OH)^+$ is further hydrolyzed to $Cd(OH)_2$, which forms a precipitate. The principal species distributions of various hydrolyzed Cd^{2+} ions reported by Srivastava et al. [23] are in the order of the following reaction:

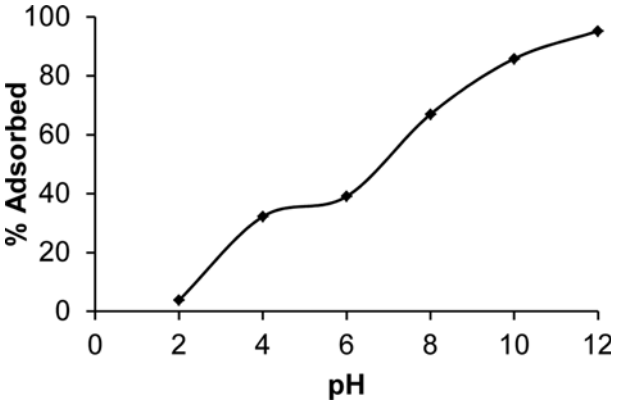

Fig. 5. Percentage of Cd^{2+} adsorbed with varying pH for CAC dosage: 0.05 mg/100 mL; rpm: 200; temperature: 30 °C; concentration: 20 mg/L).

$$Cd^{2+} + H_2O \Leftrightarrow Cd(OH)^+ + H^+, \quad pH=6 \quad (10)$$

$$Cd(OH)^+ + H_2O \Leftrightarrow Cd(OH)_2 + H^+, \quad pH=12 \quad (11)$$

Many researchers have reported that the percentage removal remains constant after pH 6 [23]. Few reports were found for Cd^{2+} removal up to pH 6 due to precipitation problem [24-26]. This is because above pH 7, the percentage removal of Cd^{2+} metal ion is due to precipitation and adsorption as reported by Srivastava et al. (2006) [23]. This would lead to inaccuracy in the prediction of percentage removal of Cd^{2+} ions. However, to find the adsorption mechanism above pH 7, the present experiment is extended up to pH 12 by removing the precipitated $Cd(OH)_2$ from the raw solution and measuring the initial and final concentration of the Cd^{2+} ions present in the solution before and after adsorption. A linear and increased percentage removal of Cd^{2+} is obtained, which confirms the increase in electrostatic attraction between the Cd^{2+} and the CAC surface. It also implies that the Cd^{2+} are more competitive to the adsorption sites than the $Cd(OH)^+$. Highest percentage removal (95%) of Cd^{2+} ions is achieved at pH 12.

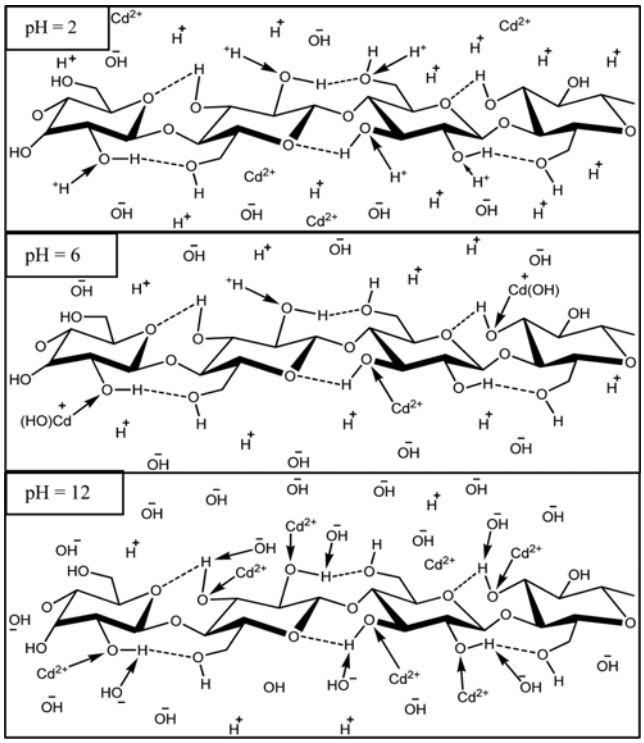

Fig. 6. Adsorption mechanism of Cd^{2+} onto CAC at pH=2, pH=6 and pH=12.

Based on the results, the adsorption mechanism of Cd^{2+} ions with the CAC adsorbent surface is proposed and presented in Fig. 6.

CONCLUSIONS

The characterization analysis of CAC proved the successful activation of *Garcinia mangostana* shell using phosphoric acid. CAC shows to have a good surface area, S_{BET} of 1,498 m^2/g with a mixture of micropores and mesopores. The adsorption of Cd^{2+} on CAC followed the Freundlich isotherm model, indicating that the adsorption sites are heterogeneous and the adsorption is multilayer. The rate of adsorption obeys second-order kinetics. From thermodynamic studies, the adsorption was found to be physisorption. The hydroxyl, carboxyl and lignin functional groups that are present on the surface of CAC played a vital role for metal binding in adsorption. pH of the metal solution also significantly influenced the metal species distribution and acid-base reactions of metal binding. The pH_{pzc} is 2.8 while the optimum pH for the adsorption of Cd^{2+} on CAC was found to be 12. Thus the present study significantly revealed the importance of surface chemistry on adsorption of metal ion.

ACKNOWLEDGEMENTS

This work is supported by High Impact Research University of Malaya (UM.C/625/1/HIR/053). The authors are grateful to NANOCEN for BET analysis, Department of Physics, University of Malaya for Zetasizer Nano particle size analyzer, FTIR, and XRD analysis.

SUPPORTING INFORMATION

Additional information as noted in the text. This information is available via the Internet at http://www.springer.com/chemistry/journal/11814.

REFERENCES

1. G. Q. Tan and D. Xiao, *J. Hazard. Mater.*, **164**, 1359 (2009).
2. J. Anandkumar and B. Mandal, *J. Hazard. Mater.*, **186**, 1088 (2011).
3. Y. C. Sharma and Uma, *J. Chem. Eng. Data*, **55**, 435 (2009).
4. J. Anandkumar and B. Mandal, *Asia-Pac. J. Chem. Eng.*, **7**, 928 (2012).
5. Y. D. Chen, B. A. Huang, M. J. Huang and B. G. Cai, *J. Taiwan Inst. Chem. Eng.*, **42**, 837 (2011).
6. S. F. Lo, S. Y. Wang, M. J. Tsai and L. D. Lin, *Chem. Eng. Res. Des.*, **90**, 1397 (2012).
7. K. Y. Foo and B. H. Hameed, *Chem. Eng. J.*, **180**, 66 (2012).
8. Y. L. Kang, S. K. S. Toh, P. Monash, S. Ibrahim and P. Saravanan, *Asia-Pac. J. Chem. Eng.*, (2013). DOI:10.1002/apj.1725.
9. R. Zein, R. Suhaili, F. Earnestly, Indrawati and E. Munaf, *J. Hazard. Mater.*, **181**, 52 (2010).
10. P. Larkin, *IR and raman spectroscopy; principles and spectral interpretation*, Elsevier, Oxford (2011).
11. P. X. Sheng, Y. P. Ting, J. P. Chen and L. Hong, *J. Colloid Interface Sci.*, **275**, 131 (2004).
12. A. M. Puziy, O. I. Poddubnaya, R. P. Socha, J. Gurgul and M. Wisniewski, *Carbon*, **46**, 2113 (2008).
13. K. Y. Foo and B. H. Hameed, *Chem. Eng. J.*, **187**, 53 (2012).
14. K. S. W. Sing, D. H. Everett, R. A. W. Haul, L. Moscou, R. A. Pierotti, J. Rouquerol and T. Siemieniewska, *Pure Appl. Chem.*, **57**, 603 (1985).
15. H. Deng, J. J. Lu, G. X. Li, G. L. Zhang and X. G. Wang, *Chem. Eng. J.*, **172**, 326 (2011).
16. A. Ahmad, M. Rafatullah, O. Sulaiman, M. H. Ibrahim and R. Hashim, *J. Hazard. Mater.*, **170**, 357 (2009).
17. F. Haghseresht and G. Q. Lu, *Energy Fuels*, **12**, 1100 (1998).
18. S. Gueu, B. Yao, K. Adouby and G. Ado, *Int. J. Environ. Sci. Technol.*, **4**, 11 (2007).
19. E. Demirbas, N. Dizge, M. T. Sulak and M. Kobya, *Chem. Eng. J.*, **148**, 480 (2009).
20. H. Lalhruaitluanga, K. Jayaram, M. N. V. Prasad and K. K. Kumar, *J. Hazard. Mater.*, **175**, 311 (2010).
21. M. F. R. Pereira, S. F. Soares, J. J. M. Orfao and J. L. Figueiredo, *Carbon*, **41**, 811 (2003).
22. C. A. L. Y. Leon, J. M. Solar, V. Calemma and L. R. Radovic, *Carbon*, **30**, 797 (1992).
23. V. C. Srivastava, I. D. Mall and I. M. Mishra, *Chem. Eng. J.*, **117**, 79 (2006).
24. P. Mavros, A. I. Zouboulis and N. K. Lazaridis, *Environ. Technol.*, **14**, 83 (1993).
25. P. Ricou, I. Lecuyer and P. Le Cloirec, *Environ. Technol.*, **19**, 1005 (1998).
26. F. A. Abu Al-Rub, M. H. El-Naas, F. Benyahia and I. Ashour, *Process Biochem.*, **39**, 1767 (2004).

Supporting Information

Surface chemistry and adsorption mechanism of cadmium ion on activated carbon derived from *Garcinia mangostana* shell

Yee Li Kang*, Mei Yi Poon*, Purushothaman Monash, Shaliza Ibrahim*, and Pichiah Saravanan*,†**

*Environmental Engineering Laboratory, Department of Civil Engineering, University of Malaya, Kuala Lumpur 50603, Malaysia
**Department of Chemical Engineering, University of Malaya, Kuala Lumpur 50603, Malaysia
(*Received 23 January 2013 • accepted 17 July 2013*)

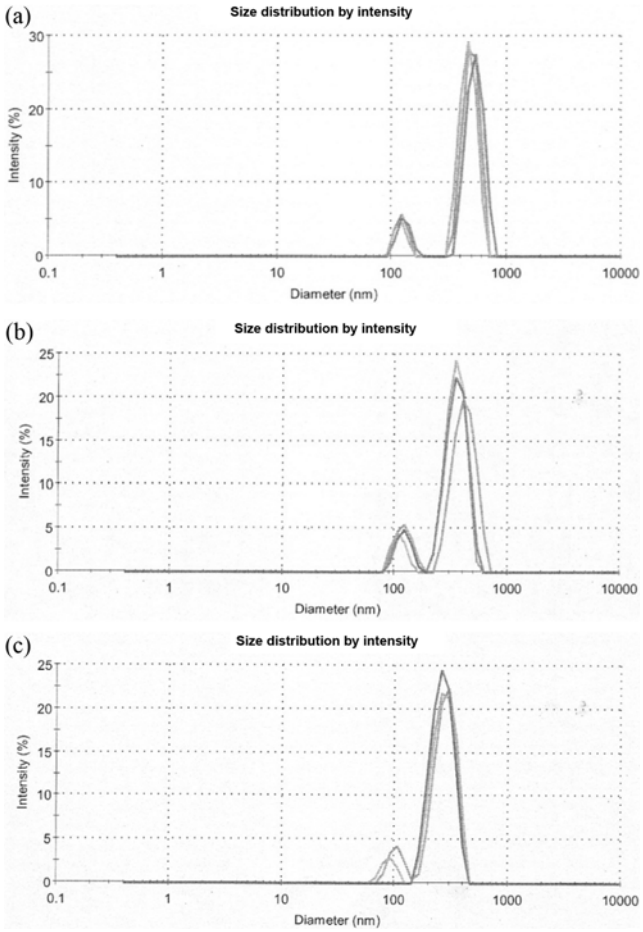

Fig. S1. Particle size distribution for (a) MS (b) char and (c) CAC.

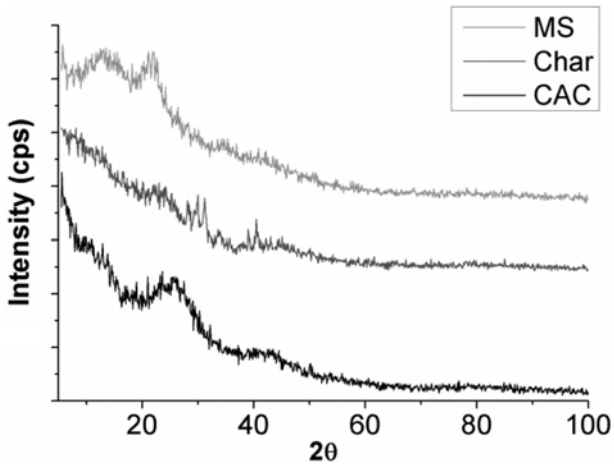

Fig. S2. XRD spectrum of the MS, char and CAC.

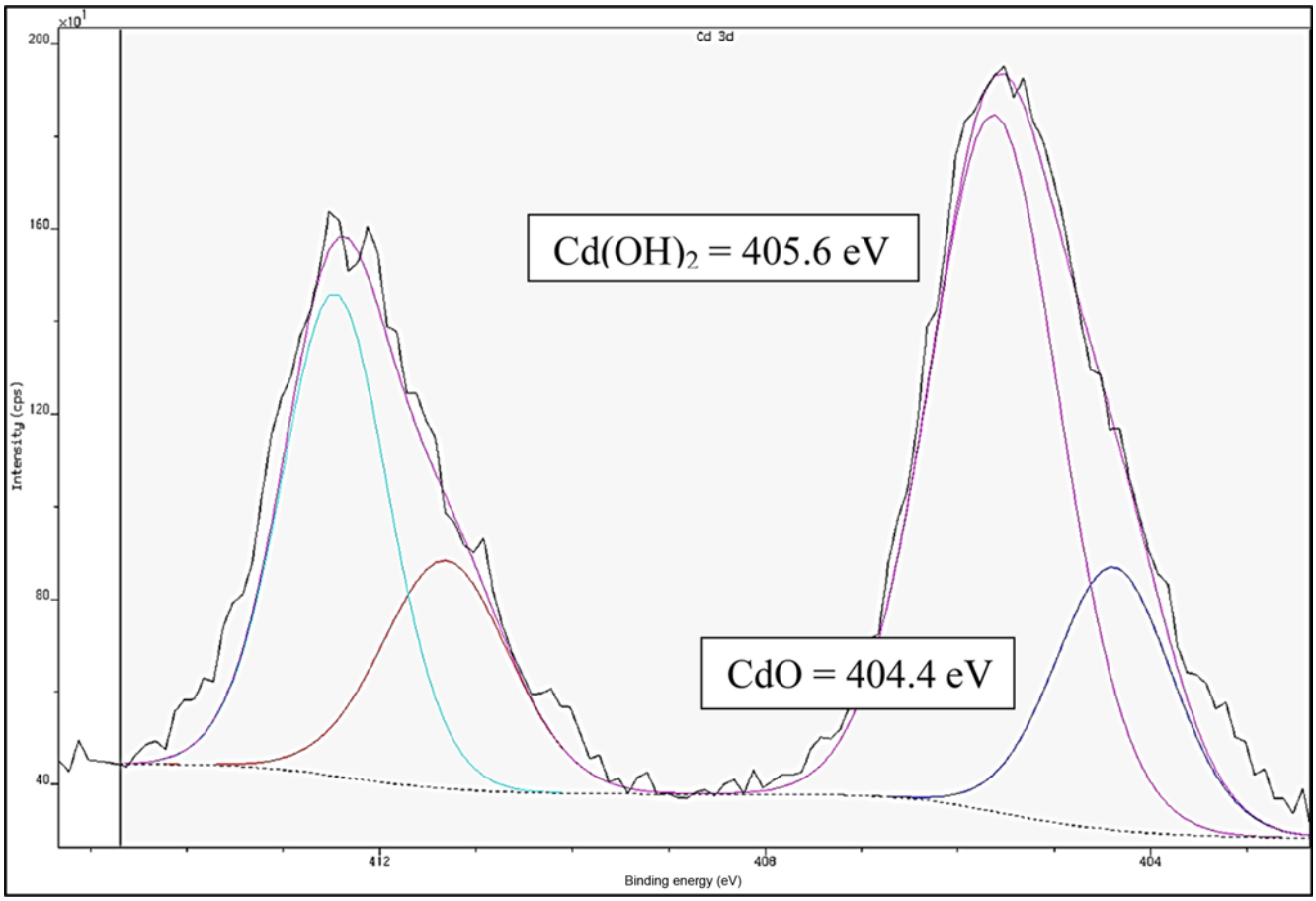

Fig. S3. XPS spectrum of Cd 3d for CAC.

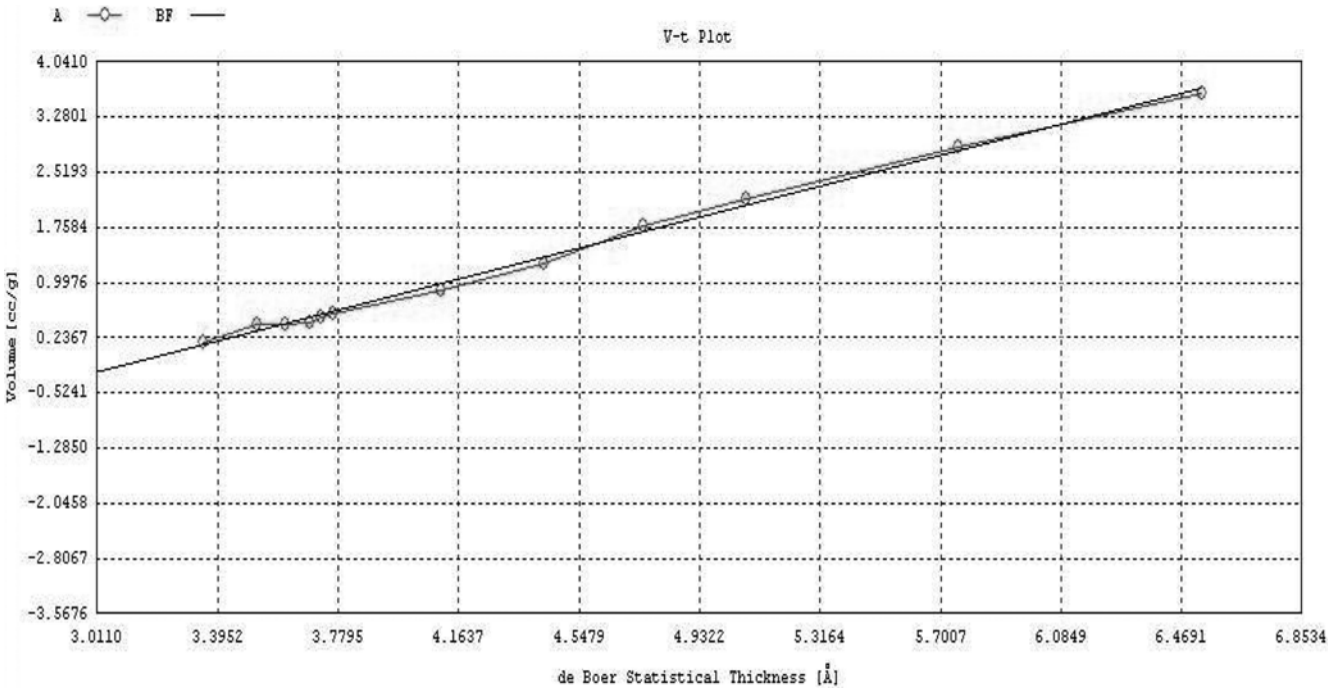

Fig. S4. t-Plot of MS.

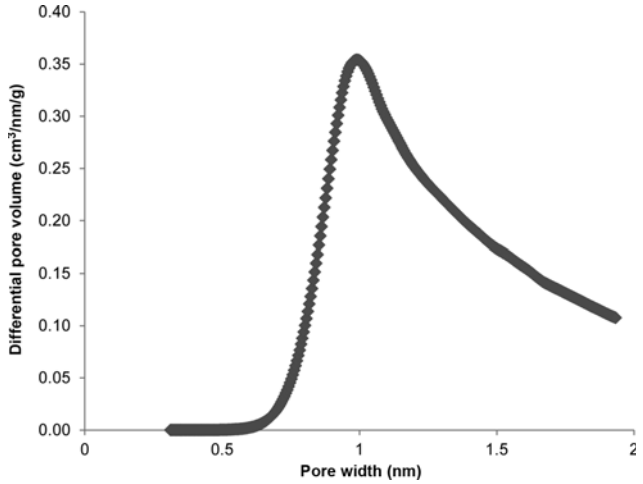

Fig. S5. Differential pore volume distributions for micropores determined by HK model for CAC.

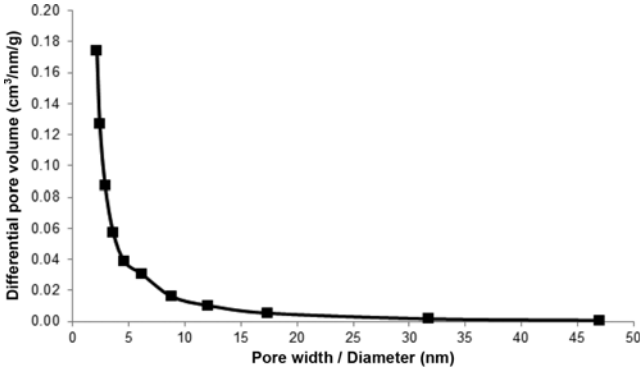

Fig. S6. Differential pore volume distributions for mesopores determined by BJH model for CAC.

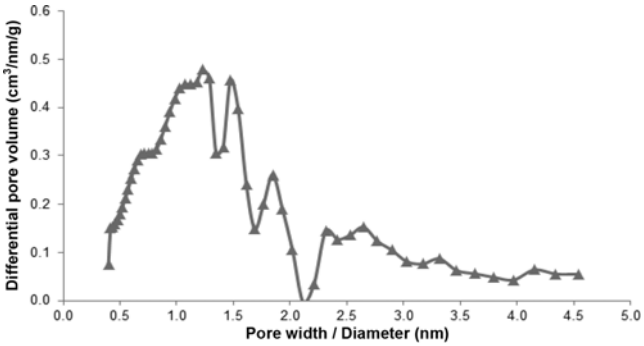

Fig. S7. Differential pore volume distributions determined by DFT model for CAC.